Mesostructured Fluids. 2. Microstructure and Supra-aggregation

ARTICLE *in* THE JOURNAL OF PHYSICAL CHEMISTRY B · OCTOBER 1999

Impact Factor: 3.3 · DOI: 10.1021/jp991243k

Mesostructured Fluids. 2. Microstructure and Supra-aggregation

I. Lisiecki,[†,‡] P. André,[†,‡] A. Filankembo,[†] C. Petit,[†,‡] J. Tanori,[‡] T. Gulik-Krzywicki,[§] B. W. Ninham,[||] and M. P. Pileni*[,†,‡]

Laboratoire SRSI, URA CNRS 1662, Université P. et M. Curie (Paris VI), B.P. 52, 4 Place Jussieu, F-752 31 Paris Cedex 05, France, CEA-CEN Saclay, DRECAM-SCM, F-91191 Gif-sur-Yvette, Cedex, France, Centre de Génétique Moléculaire-CNRS, F-91190 Gif-sur-Yvette, Cedex, France, and Department of Applied Mathematics, P.O. Box 4, Canberra, ACT, Australia 0200 and Physical Chemistry I, P.O. Box 124, University of Lund, Lund SE 22100, Sweden

Received: April 15, 1999; In Final Form: July 13, 1999

The phase behavior and microstructure of copper(II) bis(2-ethylhexyl) sulfosuccinate, $Cu(AOT)_2$−isooctane−water, is determined over a wider domain than previously used. It is characterized by a rich variety of phases and microstructures. Equilibrium phases consisting of spontaneous thermodynamically stable emulsions in equilibrium with other microstructure phases are observed. These spontaneous emulsions are composed of supra-aggregates, lamellar spherulites in which the interior and exterior are phases of interconnected cylindrical nanostructures. In another part of the phase diagram, clumps of interdigitated micelles are surrounded by an interconnected cylinder phase. The phase boundaries emerge qualitatively from elementary considerations that require only notions of local and global packing constraints.

1. Introduction

This work is a continuation of the preceding paper. The phase behavior and microstructure mixtures containing surfactants have been the subject of much confusion.[1,2] For example, some have claimed that ternary microemulsions could not exist without cosurfactant and/or made a distinction between reverse micelles and microemulsions. Similarly, with binary systems (surfactant−water), it has been maintained that single-walled vesicles are necessarily a metastable state of self-organization. All three claims are incorrect. Most of the ideas on self-assembly based on notions of local or spontaneous curvature of a surfactant film and its elastic resistance to bending together with global packing constraints have been confined to uniform structures,[1−14] for example, the ternary system DDAB/water/alkane that forms a perfect microporous media, the phase boundaries and microstructure of which vary continuously and (sometimes discontinuously) throughout a single L_2.[15] But, for any given volume fraction of components within that phase, the microstructure is homogeneous. There have been some indications that very different microstructures heterogeneous on a hundred nanometers scale can exist. Spontaneous vesicles in a surfactant−water system with an interior containing micelles are separated from an aqueous phase by a few bilayers. This concept of supra-aggregation, if established, is clearly important and adds a new dimension to the way we think about self-assembly and the notion of phases.

For the ternary system, DDAB/water/alkane mixtures,[3−5] the microstructure and phase boundaries were shown to emerge from notions of local curvature set by the balance of forces at the surfactant interface and global packing constraints. For this system, the surfactant, insoluble in both oil and water, necessarily resides at the oil−water interface. This enabled some simplifications to be made. However, the sodium−AOT system,[1] another double-chained surfactant, appeared to be quite different in its phase behavior. This apparent conflict has caused much confusion. (All these systems are crucially dependent on the counterion, which determines local curvature at the interface.)

Divalent bis(2-ethylhexyl) sulfosuccinate, $X(AOT)_2$, has been largely used these last 10 years. The first paper published in the field was by our group. Petit et al.[16] demonstrated that at low water content spherical reverse micelles are formed. With increasing water content, spherical water in oil droplets turn into cylinders. This has been done for $Cu(AOT)_2$, $Co(AOT)_2$, and $Cd(AOT)_2$. This study has been extended by other groups: Eastoe et al.[17−20] confirm the data obtained in our group and extend this to other surfactants such as $Zn(AOT)_2$, $Ni(AOT)_2$, and $(C_7H_{14})_4N(AOT)_2$. With $Mg(AOT)_2$, $Ca(AOT)_2$, and $NH_4(AOT)_2$, only spherical objects have been observed.[17] Very recently, infrared and dielectric experiments of $Ca(AOT)_2$[21] have been explained in terms of reorientation of the whole micellar aggregate and the free rotational diffusion of the completely hydrated AOT headgroups. Because these surfactants have to be synthesized, most of the study has been made in the short domain of the phase diagram, mainly in the oil rich and low water content areas. A first attempt to describe the phase diagram was done 2 years ago for $Cu(AOT)_2$.[22] It has been shown that the phase diagram is very rich. The first part of the phase diagram, at low water content, was rather well explained. The major parameter that plays a role on the change of the phase diagram is due to the change in hydration headgroup that induces an increase in the head polar area. In this present paper, it is shown that this is predictable for elementary notions.

Copper nanoparticles[23−29] formed within these mesostructured fluids have the same structure as the liquid template. The results have important implications for the meaning and definition of phases.

* All correspondence to this author.
† Université P. et M. Curie.
‡ DRECAM-SCM.
§ Centre de Génétique Moléculaire-CNRS.
|| Department of Applied Mathematic and University of Lund.

10.1021/jp991243k CCC: $18.00
Published on Web 10/28/1999

In these two papers was given a quantitative study of this phase diagram: In the preceding paper we presented the phase diagram of the $Cu(AOT)_2$/isooctane/water system and analyzed its microstructure in the low water content oil rich region. The hydrated headgroup area and the surfactant vary continuously with water content, and this adds a new complexity to the phase behavior and microstructure. In the present paper we focus attention, again on the oil region of the phase diagram, but in a domain in which the average polar headgroup is totally hydrated and remains constant. The phase behavior of $Cu(AOT)_2$/isooctane/water is extraordinary complex, with various phase regions, in each of which microstructure varies continuously with component ratios. Within each region there occur one-, two-, and three-phase regions. We demonstrate the existence of thermodynamically stable states of supra-self-assemblies, supra-aggregates. Spontaneous emulsions are formed and can be expected. A variety of phases heterogeneous at the micrometer scale exist and can be predicted from straightforward theoretical analysis.

The characterization of the phase diagram has been done by small-angle X-ray scattering (SAXS) conductivity and freeze fracture electron microscopy (FFEM). The experimental procedures are the same as in the preceding paper.

2. Theoretical Considerations

In the previous paper, which deals with microstructure in the water poor region, we have analyzed the geometrical constraints that must be satisfied by spheres and cylinders in various packing structures. It was there shown that elementary packing constraints are the overwhelming determinant of aggregate structure. Here the headgroup area of the surfactant varies with water content, and theory and experiments agree.

We now proceed to regions of the phase diagram where the polar headgroup is totally hydrated and remains constant. Supra-aggregates are formed, and taking into account some more complicated geometry constraints, their formation can be predicted. The analysis exploits the low solubility of $Cu(AOT)_2$ in isooctane and its location at the oil−water interface.

Before proceeding to the necessary analysis, we need to list here some theoretical preliminaries (for details, see the preceding paper).

The following parameters and results will be needed.

The water content, w,

$$w = \frac{N_w}{N_s} \tag{1}$$

where N_w and N_s are the number of water and surfactant molecules, respectively.

Similarly, $\bar{w}$ is defined as

$$\bar{w} = \frac{\phi_w}{\phi_s} = \frac{N_w v_w}{N_s v_s} = w\frac{v_w}{v_s} \tag{2}$$

where v_w, v_s, ϕ_w, and ϕ_s are the volume of water molecules and the surfactant and the water and surfactant volume fractions, respectively.

$$s = \frac{v_s}{a_s l_s} \tag{3}$$

Two types of packing are assumed.

(i) Packing of Spheres. For a simple cubic packing, we have

$$\phi_o^b + \phi_s + \phi_w < \frac{\pi}{6} \tag{4}$$

where ϕ_o^b is the "bound" oil volume fraction in "dressed" micelles. Bound oil is the fraction of oil taken up by surfactant tails. Then

$$\phi_s < \frac{\pi}{6}\frac{(\bar{w}s)^2 s}{\left(\bar{w}s + \frac{1}{3}\right)^3} = X_s^{s\cdot c} \tag{5}$$

$$\phi_w < \frac{\pi}{6}\frac{(\bar{w}s)^3}{\left(\bar{w}s + \frac{1}{3}\right)^3} = X_w^{s\cdot c} \tag{6}$$

The parameter $\pi/6 \approx 0.52$ can be replaced by $\sqrt{3}\pi/8 \approx 0.68$ or $\pi/3\sqrt{2} \approx 0.74$ for a body-centered cubic (bcc) or face-centered cubic (fcc) packing, respectively.

(ii) Packing of Cylinders. The cylinders can pack into **a** square structure if

$$\phi_o^b + \phi_s + \phi_w < \frac{\pi}{4} \tag{7}$$

This gives

$$\phi_s < \frac{\pi}{4}\frac{\bar{w}s^2}{\left(\bar{w}s + \frac{1}{2}\right)^2} = X_s^{c\cdot s} \tag{8}$$

$$\phi_w < \frac{\pi}{4}\frac{\bar{w}s^2}{\left(\bar{w}s + \frac{1}{2}\right)^2} = X_w^{c\cdot s} \tag{9}$$

For cylinders in hexagonal, interconnected fcc, and interconnected simple cubic (sc) structure, the parameter $\pi/4 \approx 0.78$ has to be replaced by $\pi/2\sqrt{3} \approx 0.91$, 0.82, and 0.94, respectively.

2.1. Spherulites. In this region of the phase diagram, the polar heads are totally hydrated. They form when cylinders can no longer pack.

2.1.1. Conditions for Lamellar Phases (Spontaneous Emulsions). If enough free oil exists to fill the free volume between the dressed cylinders, interactions between aggregates set the amount of free oil in the appropriate single phase. This will be generally in equilibrium with excess oil. With further addition of water, more oil is taken up, and the conditions (8) and (9) are violated. Global packing constraints demand that the system must rearrange into multilamellar structures. The amount of oil, water, and surfactant contained in these structures is again dictated by interlamellar forces.

2.1.2. Packing of Lamellae and Emulsion Droplets. We shall need to consider also the packing of multiwalled structures. Consider the structure shown in Figure 1. The water core radius, the water spacing, the thickness of free oil, and the bilayer thickness are given by R_w, L, Δ, and $d = 2l_s + \Delta + L$, respectively, where l_s is the surfactant tail length.

The water volumes in the core, first, second, ... layers of water are

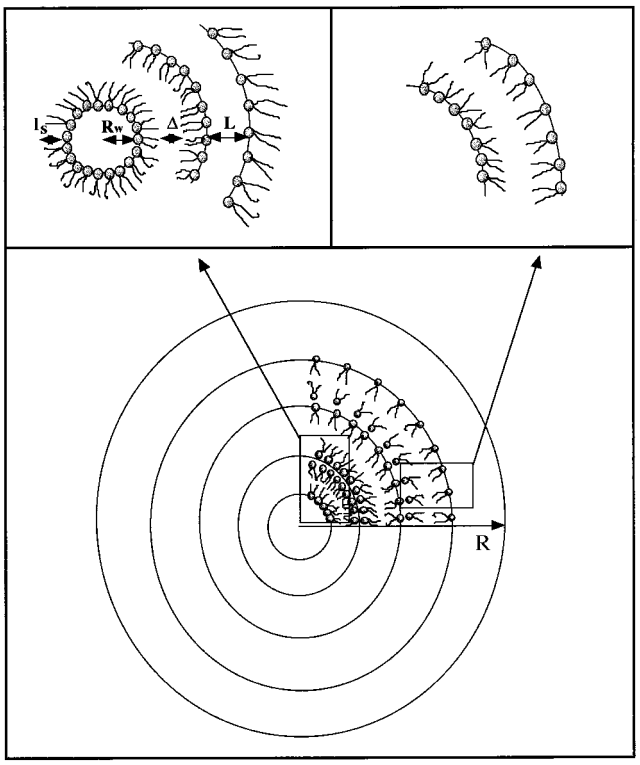

Figure 1. Characteristic parameters of spherulites.

$$\frac{4}{3}\pi R_w^3 \quad \frac{4}{3}\pi[(R_w + 2l_s + \Delta + L)^3 - (R_w + 2l_s + \Delta)^3]$$

$$\frac{4}{3}\pi\{[R_w + 2(2l_s + \Delta) + 2L]^3 - [R_w + 2)(2l_s + \Delta) + L]^3$$

...

Assuming the volume of the core can be neglected, the total volume of water contained in an onion of M layers is

$$V'_w \cong \frac{4}{3}\pi\sum_{j=1}^{M}\{[j(2l_s + \Delta) + jL]^3 - [j(2l_s + \Delta) + (j-1)L]^3\}$$

Replacing the sum by an integral, we have

$$V'_w \cong \frac{4}{3}\pi\int_{j=1}^{M}\{[j(2l_s + \Delta) + jL]^3 - [j(2l_s + \Delta) + (j-1)L]^3\}\,\mathrm{d}j$$

$$V'_w \cong \frac{4}{3}\pi\left\{(2l_s + \Delta + L)^3\frac{M^4}{4} - \frac{[(2l_s + \Delta + L)M - L]^4}{4(2l_s + \Delta + L)}\right\}$$

For large spherulites (M large) the first term is neglected. Then

$$V'_w \cong \frac{4}{3}\pi[M^3L(2l_s + \Delta + L)^2]$$

The corresponding volumes of surfactant plus any bound oil will be

$$V'_s + V'^{b}_o = \frac{2l_s}{L}V'_w$$

$$\phi_s = \frac{2l_s}{L}\phi_w = \frac{1}{\bar{w}}\phi_w \qquad (10)$$

and the volume of free oil, V'_f, is

$$V'_f = \frac{\Delta}{L}V'_w$$

$$\phi_o = \frac{\Delta}{L}\phi_w \qquad (11)$$

The surfactant parameter, s (eq 3), is close to unity ($v_s = 639$ Å^3, the hydrocarbon volume is less than this, $l_s = 10$, $a_s = 55$ Å^2). Hence the planar bilayer contains essentially no oil, with V'^{b}_o approximately zero, as expected. All oil in the lamellae is free oil.

2.1.3. Energetics of Spherulites. Assume the formation of the lamellar structures is a result of global packing constraints alone, insofar as cylinders have reached the closed packing limit (eq 9). There is now a further consequence. Internal layers will be unstable and the interior must, once formed, collapse into more complex aggregates than those we have considered so far. This is because the internal and external layers of an individual bilayer cannot satisfy the energetic constraints demanded. The matter is, in general, exceedingly complex and has been considered in greater depth previously.[11]

To illustrate how the collapse occurs, a multilamellar vesicle is considered (Figure 1), with a chain length differing with the oil−water curvature: the inner surfactant chains tend to splay with a characteristic length, l^i_s, whereas the outer layer chains tend to stretch to a maximum length, l^o_s.

The area of the internal monolayer is

$$4\pi R^2 = N^i_s a^i_s$$

The area of the outer layer is

$$4\pi(R + l^i_s + l^o_s + \Delta)^2 = N^o_s a^o_s$$

where the subscripts o and i refer to inner and outer layers. Then

$$\frac{N^o_s a^o_s}{N^i_s a^i_s} = \left(1 + \frac{l^o_s + l^i_s + \Delta}{R}\right)^2 \qquad (12)$$

The volume of the internal monolayer is

$$N^i_s v^i_s = \frac{4}{3}\pi[(R + l^i_s)^3 - R^3]$$

The volume of the outer layer is

$$N^o_s v^o_s = \frac{4}{3}\pi[(R + l^i_s + l^o_s + \Delta)^3 - (R + l^i_s + \Delta)^3]$$

Hence

$$\frac{N^o_s v^o_s}{N^i_s v^i_s} = \frac{(R + l^i_s + \Delta)^2 l^o_s\left[1 + \dfrac{l^o_s}{R + l^i_s + \Delta} + \dfrac{1}{3}\left(\dfrac{l^o_s}{R + l^i_s + \Delta}\right)^2\right]}{R^2 l^i_s\left[1 + \dfrac{l^i_s}{R} + \dfrac{1}{3}\left(\dfrac{l^i_s}{R}\right)^2\right]}$$

Assuming R is much greater than $(l^o_s + l^i_s + \Delta)$, this equation gives

$$\frac{N^o_s v^o_s}{N^i_s v^i_s} = \frac{l^o_s}{l^i_s}\left(1 + \frac{l^o_s + l^i_s + 2\Delta}{R} + \ldots\right) \qquad (13)$$

From eqs 12 and 13

$$\frac{\left(\frac{v_s}{a_s l_s}\right)^o}{\left(\frac{v_s}{a_s l_s}\right)^i} = 1 - \frac{l_s^i + l_s^o}{R} + ...$$

If this change in local curvature reflected just changes in headgroup area, keeping volume and chain length per surfactant constant, the resulting change in interfacial tension due to hydrocarbon exposed to water (5×10^{-6} J·cm $^{-2}$) would be $\Delta E = (2l_s/R)5 \times 10^{-6} a_s$ J per surfactant. At 22 °C, $kT = 4 \times 10^{-21}$ J, with $a_s = 55$ Å^2 and $l_s = 10$ Å. Then $\Delta E = 150kT/R$.

For $R = 1500$ Å, this corresponds to $0.1kT$ per molecule. Because of this high value, the internal layer of such a structure would then be forced to rearrange into a more favorable packing consistent with overall volume fractions.

This difference in local curvature due to symmetry of packing can be accommodated in several ways: (i) changing headgroup area; (ii) squeezing out bound oil from the outer layer or taking up more in the inner layer; (iii) compressing the inner chains by reducing the chain length l_s^i.

All factors compiled together lead to the same conclusion. The major factor is probably (iii). If so, the occurrence of spherulites (or emulsions) as on equilibrium state of self-assembly is not expected to be universal. It depends on chain "stiffness".[11]

2.1.4. Spherulite Composition and Structure. From the volume fraction in the multilamellar structures, which are set by the global packing conditions, the nature of the interior aggregates can be explored.

From eqs 10 and 11, the interior constitution of these supra-aggregates can be estimated. Bound oil is essentially zero (see above) since the major contribution to the interior volume fraction comes from collapsed lamellae of large radius.

The peak to peak spacing, d, is

$$d = 2l_s + \Delta + L \tag{14}$$

Two factors conspire together to determine supra-aggregate structure: (i) the global packing factor demands the formation of multilamellar states (cylinders can no longer pack again); (ii) from an energetic point of view, the collapse of the interior to small aggregates is favorable.

We can estimate these from the onset conditions (eq 9) when cylinders are forbidden. At the transition, the lamellar phase and the interconnected cylinders keep the same polar volume fraction for cylinders in interconnected fcc structure. From eqs 9−11

$$\phi_w = 0.82\frac{1}{\left(1 + \frac{l_s}{sL}\right)^2} = X_w \tag{15}$$

In taking 0.82 in eq 15, we have taken a main parameter between the most loose and most compact packing of cylinders (cf. eq 9).

$$\phi_o = 1 - (\phi_w + \phi_s) = 1 - \phi_w\left(1 + \frac{1}{\bar{w}}\right)$$

Hence

$$\frac{\Delta}{L} = \frac{1}{0.82}\left(1 + \frac{l_s}{sL}\right)^2 - \left(1 + 2\frac{l_s}{L}\right) \tag{16}$$

Combining eqs 14 and 16, we obtain

$$L^2 + L\left(\frac{2l_s}{s} - 0.82d\right) + \left(\frac{l_s}{s}\right)^2 = 0 \tag{17}$$

The solution of this nonlinear equation gives the amount of water and oil within the supra-aggregate at a point in the phase diagram where spherulites exist.

2.1.5. Biphasic System Made of Spherulites in Equilibrium with the Isotropic Phase: Relation of the Volume Fraction in the Two Phases. The data presented below show a decrease in the spherulite phase with a decrease in the lamellar spacing and an increase in the isotropic phase with increasing water content.

Once spherulites form, they will phase separate; an upper single phase will remain as connected cylinders. The free space between spherulites will be filled with the same connected cylinders phase. In this region, we assume that the cylinders are interconnected. The conditions that a single phase made up of cylinders can exist, in square packing, is determined through eqs 8 and 9:

$$\phi_w^c < \frac{\pi}{4}\frac{(\bar{w}s)^2}{\left(\bar{w}s + \frac{1}{2}\right)^2} = X_w^{c\cdot s}$$

and

$$\phi_s^c < \frac{\pi}{4}\frac{\bar{w}s^2}{\left(\bar{w}s + \frac{1}{2}\right)^2} = X_s^{c\cdot s}$$

When the inequality is violated, by reducing oil, or adding water, the system is forced to pack some material into the lamellar spherullite phase or interconnected cylinders.

If the lower phase, which is denser, settles into a close-packed array of uniform spherulites (this is a crude approximation, but the result should be independent of this), one part of the solution in a volume fraction, f, is composed of a phase of cylinders alone and the other part is made of spherulites and cylinders in the free volume remaining in the lower phase.

If the packing of spherulites is simple cubic, the volume fraction of spherulites is $\pi/6 \approx {}^1/_2$. Then, half of the volume is taken by spherulite and half by the cylinder phase that fills up the gaps between the spheres.

The overall volume fractions of surfactant, oil, and water for the system are given by Φ_s, Φ_o, and Φ_w, respectively.

In the lamellae, the volume fractions are respectively $2l_s/d$, Δ/d, L/d, with the bilayer thickness $d = \Delta + L + 2l_s$.

So, if the initial state has the fractions f, $1 - f$, we have

$$\Phi_s = \left[f + \left(1 - \frac{\pi}{6}\right)(1 - f)\right]\phi_s^c + \frac{\pi}{6}(1 - f)\frac{2l_s}{d} \tag{18}$$

$$\Phi_w = \left[f + \left(1 - \frac{\pi}{6}\right)(1 - f)\right]\phi_w^c + \frac{\pi}{6}(1 - f)\frac{L}{d} \tag{19}$$

$$\Phi_o = \left[f + \left(1 - \frac{\pi}{6}\right)(1 - f)\right]\phi_o^c + \frac{\pi}{6}(1 - f)\frac{\Delta}{d} \tag{20}$$

If the spherulites are not close packed and polydispersed, the factor $\pi/6$ will be reduced. Arbitrarily, to illustrate changes in composition and structures that occur under water dilution, the factor has been reduced by 1.5.

2.2. Interdigitated Aggregates. *2.2.1. Interdigitation of Droplets Remaining Spherical.* In a first approximation it is assumed that spheres are packed in a simple cubic structure, which provides the equivalence of a single droplet and the elementary cell of the array. The equations are much more

complicated for bcc and fcc random packing. Minimal conditions for interdigitation of spheres are

$$\frac{4\pi}{3}R_w^3 = N_w v_w$$

$$4\pi R_w^2 = N_s a_s$$

which ratio gives $R_w = 3\bar{w}sl_s$ and $N_s a_s = 4\pi(3\bar{w}sl_s)^2$.

$$(2R_w + 2l_s)^3 = N_w v_w + N_s v_s + N_o v_o \qquad (21)$$

Equation 21 can be written as

$$\frac{l_s^3}{N_s v_s}\left(2\frac{R_w}{l_s} + 2\right) = \frac{N_w v_w}{N_s v_s} + 1 + \frac{N_o v_o}{N_s v_s}$$

Hence, using eqs 2 and 3 and the R_w relation and for interdigitations of spheres, the volume fraction ratio of oil and surfactant is defined as

$$\frac{\phi_o}{\phi_s} = \frac{(6\bar{w}s + 2)^3}{\pi s(6\bar{w}s)^2} - (\bar{w} + 1) \qquad (22)$$

The system has two options. It can interdigitate or go to a denser (bcc, fcc) packing as ϕ_o decreases.

2.2.2. Interdigitated Cylinders. When there is no longer sufficient excess oil to accommodate the curvature requirements of the surfactant chains, the chains must interdigitate. The minimum amount of oil volume fraction at which this process occurs can be estimated. At the boundaries of the Wigner−Seitz cell, cylinders in square packing must interdigitate and the chains interpenetrate. Some free oil is available, but not enough to fill the joint requirement of satisfying the oil demands of the tails and to fill up the gaps between the cylinders. Then the volume per unit length of cylinders is

$$\pi R_w^2 = N_w v_w \qquad (23)$$

and the surface per unit length of cylinders is

$$2\pi R_w = N_s a_s \qquad (24)$$

At the beginning of interdigitation

$$(2R_w + 2l_s)^2 = N_w v_w + N_s v_s + N_o v_o \qquad (25)$$

The ratio of eqs 23 and 24 gives

$$R_w = 2\frac{N_w v_w}{N_s a_s}$$

Using eqs 2 and 3, we have

$$R_w = 2\bar{w}sl_s \qquad (26)$$

Taking eqs 26, 2, and 3, eq 25 can be written

$$\frac{\phi_o}{\phi_s} = \frac{(2\bar{w}s + 1)^2}{\pi\bar{w}s^2} - (\bar{w} + 1) \qquad (27)$$

and clearly we must have $\phi_o > 0$.

3. Phase Behavior of the Cu(AOT)$_2$−Isooctane−Water Solution

We are now in a position to understand the system. We first give a broad outline of the phase diagram. The structural studies follow this description.

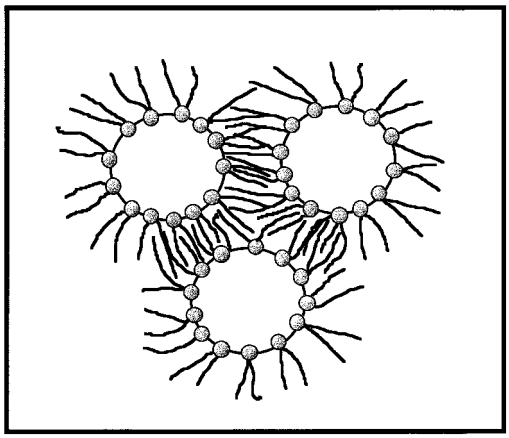

Figure 2. Interdigitate water in oil aggregates.

Each region is characterized by (i) visual inspection between crossed polarizers to give an initial characterization (number and boundaries of coexisting phases, birefringent or isotropic phases), (ii) freeze fracture electron microscopy, FFEM, (iii) conductivity measurements, and (iv) small angle X-ray scattering, SAXS.

The procedure used is the following: Cu(AOT)$_2$ was mixed with isooctane at a given concentration and water added progressively to the solution. [Samples were sealed, vigorously shaken and centrifuged. They were allowed to stand for several days. In fact, the equilibrium phase forms in a few minutes. Each sample was checked for reversibility to temperature cycles.] Region boundaries appear along lines essentially of constant water-to-surfactant ratios, corresponding to discrete jumps in headgroup area as the surfactant is progressively hydrated. The resulting ternary diagram is shown in Figure 3. Colored regions correspond to distinct macroscopic phases in equilibrium with excess isooctane. All phases are separated by very flat menisci, of ultralow interfacial tension. Hatched regions are those with no excess isooctane. Subscripts b and t indicate biphasic and triphasic regions. The notation "region" I, II, III... is used to indicate visually different phase regions. The ternary phase diagram exhibits the following features.

Let $w = [H_2O]/[[AOT]$ be the ratio of the number of water to surfactant molecules.

To simplify the notation, we consider that low surfactant concentration refers to samples of initial copper concentration equal to 1.2×10^{-1} M when high surfactant concentration refers to 4.2×10^{-1} M.

Whatever the Cu(AOT)$_2$ concentration, at very low water content, an isotropic phase is observed (region I). In the preceding paper, formation of isolated water in oil droplets, at low water content ($w = 2$) is discussed. With increasing water content ($w = 4$), elongated droplets are formed and interconnect with increasing Cu(AOT)$_2$ concentration. These changes are predicted by simple packing constraints.

With increasing water content to $w = 5$, the phase diagram depends on the Cu(AOT)$_2$ concentration: At low Cu(AOT)$_2$ concentration, an isooctane phase is in equilibrium with one or two phases. On the other hand, with increasing Cu(AOT)$_2$ concentration, the isooctane phase progressively disappears and there remain phases containing the surfactant.

Above $w = 5$, region II$_b$ is composed of an isotropic phase in equilibrium with isooctane. With an increase in water content, the isotropic phase progressively decreases. With an increase in Cu(AOT)$_2$ concentration, the isooctane volume progressively decreases to give rise to a monophasic isotropic solution. This single phase region II is reached. The isotropic phase is made

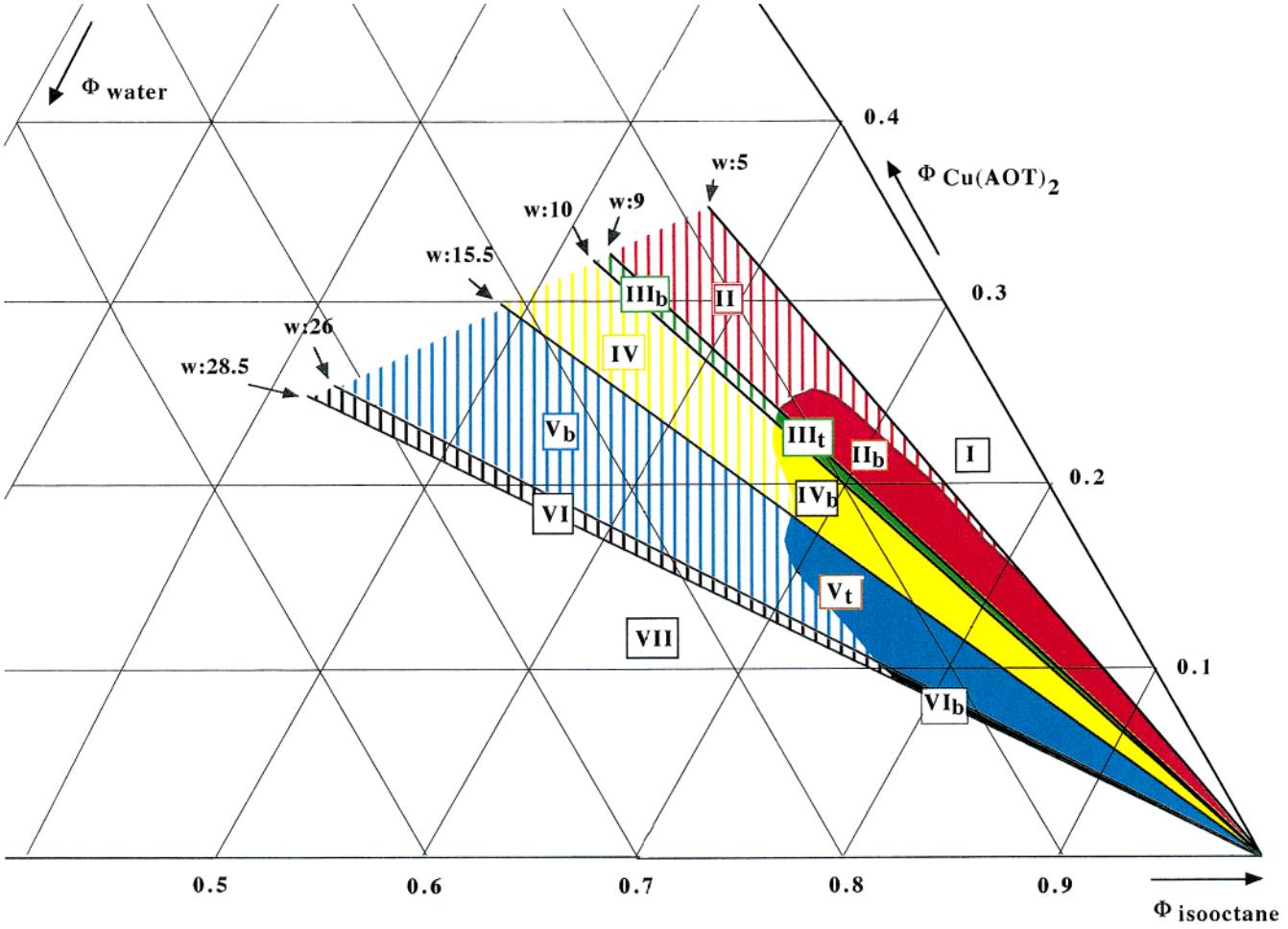

Figure 3. Phase diagram of $Cu(AOT)_2$−water−isooctane.

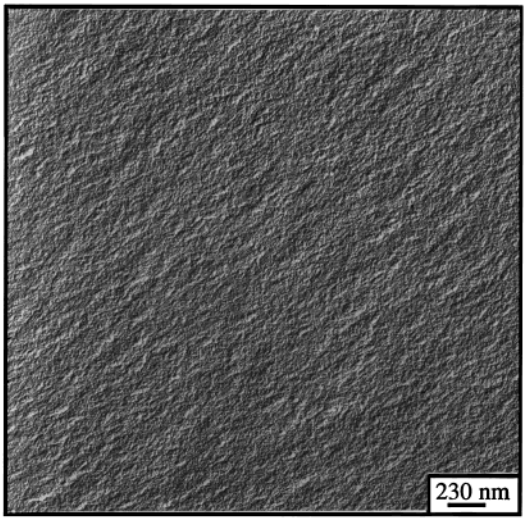

Figure 4. FFEM pattern of the isotropic phase of region II_b at $[Cu(AOT)]_2 = 1.2 \times 10^{-1}$ M, $w = 7$ ($\phi_s = 0.26$, $\phi_w = 0.09$, $\phi_o = 0.65$).

up of interconnected cylindrical droplets. The FFEM pattern of the isotropic phase of region II_b shows the presence of very small objects (Figure 4).

At $w = 9$, a birefringent phase in equilibrium with isooctane and the isotropic phase appears (region III_t). The isotropic phase is characterized by the presence of small objects, as observed in Figure 4 when the birefringent phase is a mixture of planar lamellae and spherulites (see preceding paper). With increasing $Cu(AOT)_2$ concentration, the pure isooctane phase disappears and two phases (III_b) coexist with a cloudy, but not birefringent, lower phase and an isotropic upper phase. Regions III_t and III_b exist in a very small water content range ($9 < w < 10$).

At $w = 10$, there remains only the birefringent phase in equilibrium with isooctane. Region IV_b exists in a rather large domain of w ($10 < w < 15.5$). The FFEM patterns show formation of a distorted planar lamellar phase (Figure 5A) in coexistence with an onion-like phase that we call spherulites (Figure 5B).

With increasing $Cu(AOT)_2$ concentration, less and less isooctane is released and only one birefringent phase is obtained (region IV). The FFEM pattern shows only spherulites (Figure 6).

Figure 3 shows that the boundaries between different phase regions appear as straight lines of constant w emerging from the isooctane corner. This is remarkable. It indicates that in all regions of the phase diagram, the polar headgroup area is constant for each phase region. This is confirmed below for the water rich phases.

Details of the structure of phases belonging to regions I−IV have been given in the preceding paper. We concentrate our efforts on regions V and VII.

At $w = 15.5$, an isotropic phase appears in equilibrium with the birefringent one and excess isooctane. Region V_t exists over the water content range from 15.5 to 26. When the water content is increased from 15.5 to 26, the isotropic phase progressively increases and the birefringent phase disappears. The FFEM pattern of the birefringent phase (Figure 7) shows a phase made of spherulites containing in their interiors another structure. The

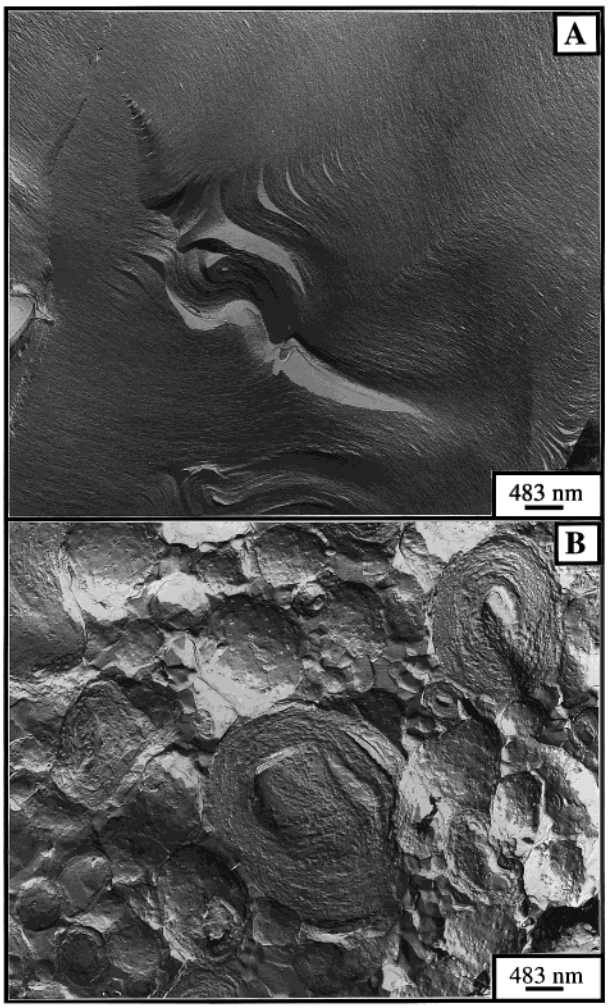

Figure 5. FFEM patterns of the birefringent phase of region IV_b at $[Cu(AOT)_2]_0 = 1.2 \times 10^{-1}$ M, $w = 12$ ($\phi_s = 0.22$, $\phi_w = 0.12$, $\phi_o = 0.66$).

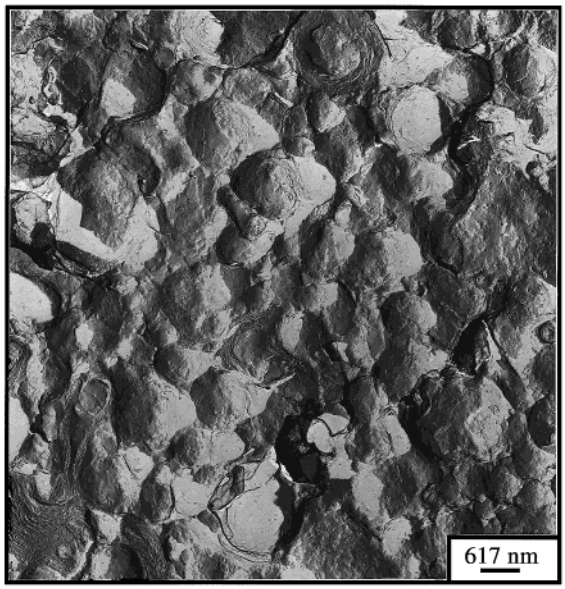

Figure 6. FFEM patterns of the birefringent phase of region IV observed at $[Cu(AOT)_2]_0 = 4.2.\ 10^{-1}$ M, $w = 12$ ($\phi_s = 0.27$, $\phi_w = 0.16$, $\phi_o = 0.57$).

interior phase looks like that observed in Figure 4 and can be assigned to interconnected cylinders (see preceding paper). On increasing $Cu(AOT)_2$ concentration, with time and/or under centrifugation, the isooctane phase progressively disappears and two well-defined phases appear: an isotropic phase (V_{b1}) and a birefringent one (V_{b2}) (region V_b). The FFEM pattern of phase V_{b1} shows small objects in equilibrium with larger ones (Figure 8A). Phase V_{b2} shows the spherulite phase made of large lamellar objects containing in both the interior and exterior interconnected cylinders (Figure 8B). This cylinder phase is the same as that observed in phase V_{b1}. The system is thermodynamically stable. On heating, the apparent two-phase system turns into a single isotropic phase. On cooling, the two "phases" appear again, in the same proportion.

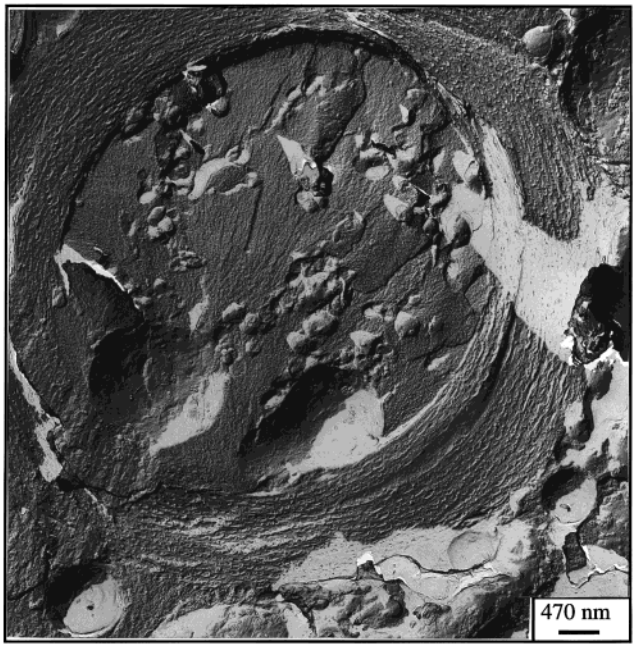

Figure 7. FFEM patterns of the birefringent phase of region V_t observed at $[Cu(AOT)_2]_0 = 1.2 \times 10^{-1}$ M, $w = 17$.

In the following, we present structural data for the isotropic (V_{b1}) and birefringent (V_{b2}) phases.

The headgroup area in phase V_{b1} is determined by SAXS experiments at various water contents, from the Porod limit of the scattering curve. Table 1 shows that it is equal to that determined at high water content for Na(AOT).

The scattering from phase V_{b1} indicates the presence of cylinders. However, because of the high concentration of surfactant, it is impossible to determine the mean chord length. The average width increases with increasing water content (Table 1). The measurement of the AOT and water concentrations permits one to calculate the water content, w', in the upper phase (phase V_{b1}). Table 2 shows that, when the water content is increased from $w = 17$ to $w = 24$, w' remains constant and is always higher than the overall water content used to make phase V_b. The conductance in the isotropic phase (V_{b1}) is rather large (in the milliSiemens scale) and increases with increasing water content (Table 1). This indicates an increase in connectivity of the cylinders on water addition. Figure 9 shows the variation, at various water contents, of the scattering intensity versus the wave vector, q. A peak due to the structure factor is observed. It is shifted toward larger q values with increasing water volume fraction, ϕ_w. The D^* value ($D^* = 2\pi/q$) is given for various water contents (Table 1).

When the packing conditions are violated, the system has to turn from spheres to cylinders (at the opposite extreme, when the volume fractions are such that spheres can pack, the

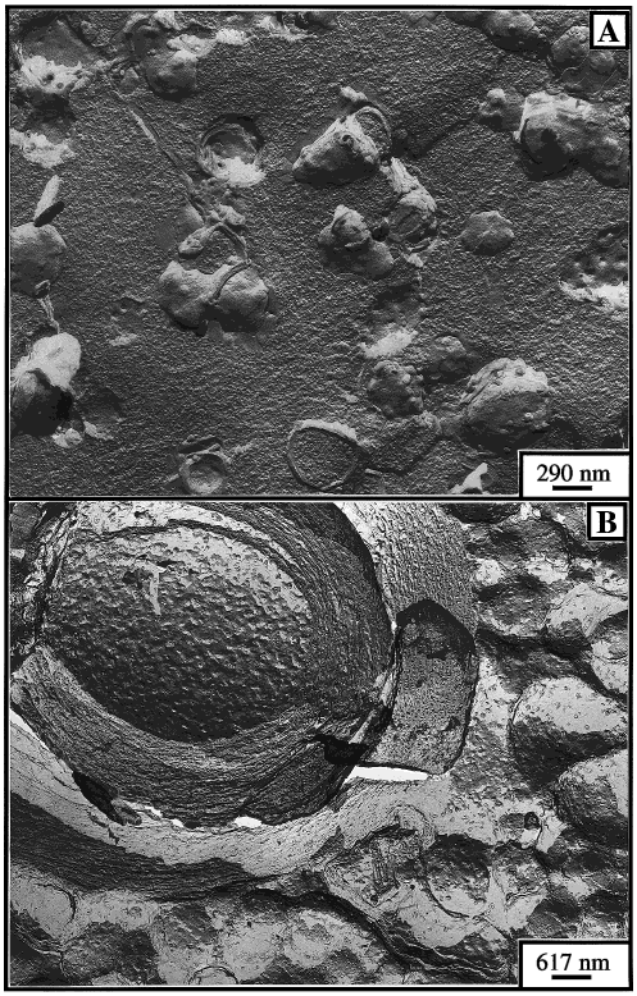

Figure 8. FFEM patterns of region V_b observed at $[Cu(AOT)_2]_0 = 4.2 \times 10^{-1}$ M, of phase V_{b1} (A), $w = 23$, and of phase V_{b2} (B), $w = 21$.

TABLE 1: For Phase V_{b1}, Overall Water Content of Region V_b, w, Head Polar Area, σ, Measured Concentration of Surfactant and Water, [AOT] and [H_2O], Shape of the Objects (Cylinders (c)), Ratio of Measured Water to Surfactant Concentration, w', and Width of the Cylinders, l^c [a]

w	17	18	19	20	21	22	23	24
σ (Å^2)	50	51	48	48	48	50	50	51
$10[AOT]_0$		4.5	4.7	5.1	5.5	5.7	6	6.1
[H_2O]		10.5	11.2	12.1	12.7	13.7	14.7	15.2
shape	c	c	c	c	c	c	c	c
w'		23.5	23.8	23.9	22.9	23.9	24.5	24.8
l^c (Å)	62	70	74	74	78	78	82	82
q_{max} (cm^{-1})	0.04	0.04	0.045	0.05	0.05	0.05	0.05	0.052
D^* (Å)	157	157	157	146	127	125	125	121
$100\phi_s$		17	18	19	21	22	23	24
$100\sigma_w$		19	20	22	23	25	27	27
$100\phi_o$		64	62	59	56	53	50	49
$\bar{w}$		1.08	1.11	1.12	1.07	1.12	1.15	1.16
κ (mS)		0.8	1.2	1.3	1.4	1.4	1.6	1.6

[a] $D^* = 2\pi/q_{max}$ when q_{max} is the maximum of the scattering intensity. Surfactant, ϕ_s, water, ϕ_w, and oil, ϕ_o, volume fractions measured from analysis of the various compounds. $\bar{w}$ is the ratio of measured water to surfactant volume fraction, and κ is the conductance of phase V_{b1}, with $[Cu(AOT)_2]_0 = 4.2 \times 10^{-1}$ M.

interactions between aggregates could induce the phase transition from spheres to cylinders). The existence of an interconnected cylinder microstructure is strongly supported by the high conductance measured in phase V_{b1}.

TABLE 2: For Phase V_{b2}, Overall Water Content of Region V_b, w, Measured Concentration of Surfactant and Water, [AOT] and [H_2O], Shape of the Objects (Lamella (l)), Ratio of Measured Water to Surfactant Concentration, w', Water Volume Fraction Deduced from the $D^* = 2\pi/q_{max}$ Position, ϕ_w^* [a]

w	17	18	19	20	21	22	23	24
$10[AOT]_0$		7.4	7.6	7.6	7.7	7.8	7.1	6.7
[H_2O]		12	12.7	12.8	13.4	13.4	12.4	12
shape		l	l	l	l	l	l	l
w'		16.3	16.6	16.7	17.5	17.3	17.5	17.8
d (Å)	72	63.5	61.9	59.3	57.6	56.1	55.6	55.1
D^* (Å)			157	140	126	125	125	125
$100\phi_w^*$			19	22	26	26	26	26
$100\phi_s$		28	29	29	30	30	27	26
$100\phi_w$		22	23	23	24	24	22	22
$100\phi_o$		50	48	48	46	46	50	53
Δ (Å)		4	4	4	4	3	3	3
L (Å)		39	38	35	34	33	32	32
$100X_w$		56	55	54	53	52	51	51

[a] Surfactant, ϕ_s, water, ϕ_w, and oil, ϕ_o, volume fractions measured. Δ and L are the thickness of oil and water in the lamellar phase. X_w is the water volume fraction of the internal phase deduced from eq 15 with $[Cu(AOT)_2]_0 = 4.2 \times 10^{-1}$ M.

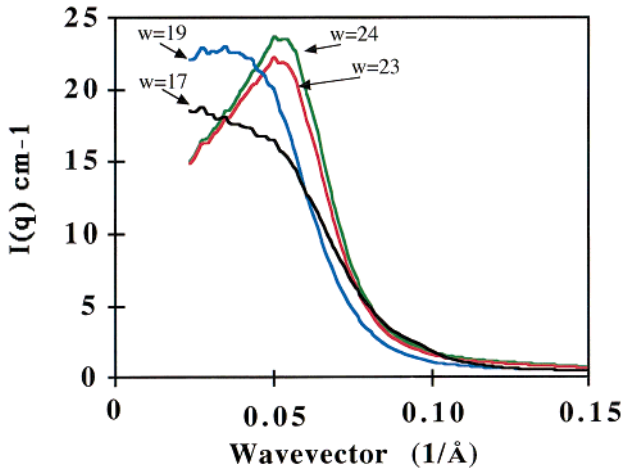

Figure 9. Variation of the X-ray scattering intensity with the q angle of the isotropic phase (phase V_{b1}), $[Cu(AOT)_2]_0 = 4.2 \times 10^{-1}$ M at various water contents: $w = 17$ (black), $w = 19$ (blue), $w = 23$ (red), and $w = 24$ (green).

Phase V_{b2} is a birefringent phase. The SAXS patterns change markedly with increasing water content. At low w value, a large Bragg peak is observed and a strong increase in the scattering intensity at low q value is observed (Figure 10). This can be related to the presence of small objects located in the interior of the spherulites and/or in the intralamellar region. With increasing water content, Figure 10 shows a decrease in the width of the Bragg peak and an increase in its intensity. From this it can be concluded that the increase in water content induces an increase in the ordering of the lamellar phase (fluctuations are damped). Furthermore, the increase in the water content induces a shift toward large q values of the Bragg peak. This indicates a decrease in the interlamellar distance, d, with increasing water content (Table 2). Figure 10 shows the progressive emergence of a new peak with increasing water content. The position of this new peak is in the same range as the q values observed in the isotropic phase (Figure 9). This indicates that the birefringent phase contains the same isotropic phase. This is consistent with the FFEM pattern obtained for phase V_{b2} (Figure 8B) where spherulites are surrounded by small objects and have similar objects in their interiors. Taking into account the fact that the isotropic phase is made of intercon-

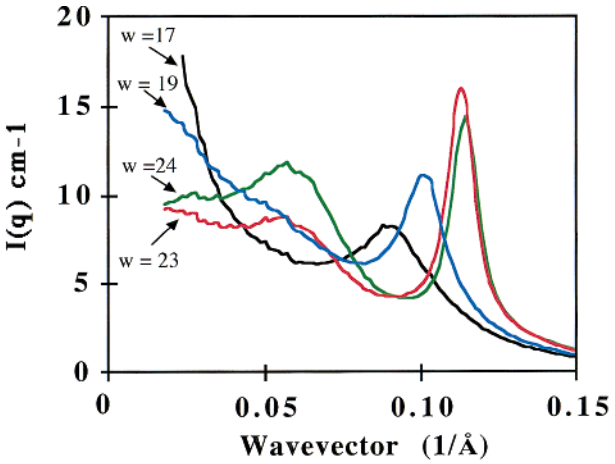

Figure 10. Variation of the X-ray scattering intensity with the q angle of the birefringent phase (phase V_{b2}), $[Cu(AOT)_2]_0 = 4.2 \times 10^{-1}$ M at various water contents: $w = 17$ (black), $w = 19$ (blue), $w = 23$ (red), and $w = 24$ (green).

TABLE 3: Overall Data for Region V_b, Water Content, w, Volume of the Isotropic Phase (Phase V_{b1}), $V_{isotrope}$, Volume of the Birefringent Phase (Phase V_{b2}), $V_{birefringente}$, Volume Fraction, ϕ[a]

w	18	19	20	21	22	23	24
$V_{isotrope}$ (mL)	0.71	1.11	1.64	2.21	2.56	2.83	3.16
$V_{birefringente}$ (mL	2.99	2.18	2.22	1.70	1.36	1.15	0.87
$f = 100V_{isotrope}/V_{total}$	19	30	43	57	65	71	78
$100\Phi_s(exp)_0$	26	26	25	25	25	24	24
$100\Phi_w(cal)_0$	21	22	22	23	24	24	25
$100\Phi_w(exp)_0$	21	22	22	23	24	24	26
$100F_o(cal)_0$	29	29	28	28	28	29	29
$100F_o(exp)_0$	53	52	53	52	51	50	50
$100F_o(cal)_0$	50	50	49	49	48	46	46

[a] Overall surfactant, $\Phi_s(exp)$, water, $\Phi_w(exp)$, and oil, $\Phi_o(exp)$, volume fractions determined from the measure of the various compounds of the phase. Overall surfactant, $\Phi_s(cal)$, water, $\Phi_w(cal)$, and oil, $\Phi_o(cal)$, volume fractions calculated from eqs 18−20. $[Cu(AOT)_2]_0 = 4.2 \times 10^{-1}$ M.

nected cylinders, these small objects are probably the same. Hence from SAXS and FFEM patterns, it can be concluded that the birefringent phase does indeed contain an isotropic one.

If we assume that the peak is due to the isotropic phase within the birefringent phase (phase V_{b2}), the water volume fraction, ϕ_w*, of the isotropic phase contained in the birefringent one can be deduced from the SAXS measurements. As matter of fact, Table 1 shows a decrease in the D* value with increasing water volume fraction, ϕ_w. From the D* assigned to the isotropic phase within the birefringent one (Figure 10), its water volume fraction, ϕ_w*, can be deduced at various water contents. Table 2 shows that the ϕ_w* increases from 0.19 to 0.26, with increasing w. In the isotropic phase (phase Vb1), the measured water volume fraction, ϕ_w, increases with water content (Table 1). Comparison of Tables 1 and 2 shows the same average values of ϕ_w and ϕ_w*. This confirms again that the birefringent phase contains the isotropic one with the same composition. Taking into account that these two phases (V_{b1} and V_{b2}) are obtained by two routes, either under centrifugation or with time, we could reasonably conclude that the spherulites contain an isotropic phase in both interior and exterior phases.

The various parameters of the two phases (V_{b1} and V_{b2}) change considerably with increasing overall water content, w, from 17 to 26:

(i) Phase V_{b1} shows an increase of its volume, of the water content, w', and of the surfactant, ϕ_s, and the water, ϕ_w, volume fractions (Tables 1 and 3).

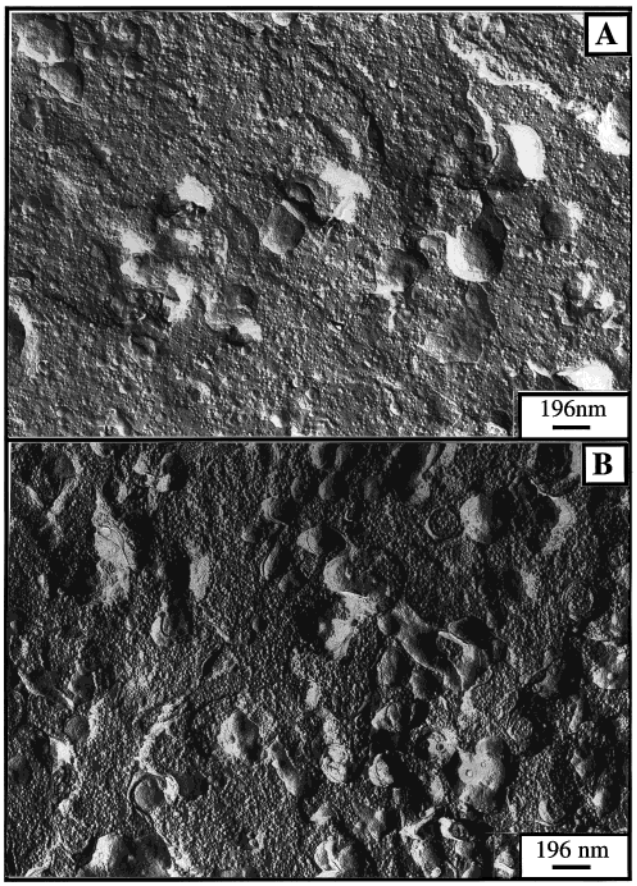

Figure 11. FFEM patterns of isotropic phases of regions VI_b ($\phi_s = 0.09$, $\phi_w = 0.13$, $\phi_o = 0.78$) (A) and VI ($\phi_s = 0.23$, $\phi_w = 0.29$, $\phi_o = 0.48$) (B) observed at $w = 26.5$ and $[Cu(AOT)_2]_0 = 1.2 \times 10^{-1}$ M and $[Cu(AOT)_2]_0 = 4.2 \times 10^{-1}$ M.

TABLE 4: For Region VII, Head Polar Group Area, σ, Shape of the Objects (Cylinders (c) or Spheres (s)), Polar Radius of Spherical Droplet, R^s, Length of the Cylinders, L^c, Width of the Cylinders, l^c, Surfactant, ϕ_s, Water, ϕ_w, and Oil, ϕ_o, Volume Fractions Measured[a]

w	29	30	31	32	33	34	35	36	37	38
σ (Å^2)		50		55		50		55		
shape		c		c/s		s		s		
R^s(Å)				60		65		70		
L^c (Å)		150								
l^c (Å)		110								
$100\phi_s$	8.2	8.2	8.1	8.1	8.1	8.1	8.0	8.0	8.0	7.9
$100\phi_w$	11.1	11.5	11.8	12.1	12.5	12.8	13.1	13.5	13.8	13.9
$100\phi_o$	80.7	81.3	80	79.7	79.4	79.1	78.8	78.5	78.3	78.1
ϕ_o/ϕ_s(exp)	9.83	9.83	9.83	9.83	9.83	9.83	9.83	9.83	9.83	9.83
ϕ_o/ϕ_s(cal s)	2.25	2.28	2.31	2.34	2.37	2.41	2.44	2.47	2.51	2.54
ϕ_o/ϕ_s(cal c)	0.64	0.65	0.65	0.66	0.67	0.68	0.69	0.70	0.70	0.71

[a] ϕ_o/ϕ_s(cal s) and ϕ_o/ϕ_s(cal c): calculated ratio of oil versus surfactant volume fraction for interdigitated spheres and cylinders, respectively. $[Cu(AOT)_2]_0 = 1.2 \times 10^{-1}$ M.

(ii) Phase Vb2 shows a corresponding decrease in volume, of the water content, w', and of the surfactant, ϕ_s, and the water, ϕ_w, volume fractions (Tables 2 and 3). The spacing of the lamellae decreases, whereas the order of the lamellae increases.

(iii) The isotropic phase within the lower phase (V_{b2}) has the same composition as that of the upper phase (V_{b1}).

From these data, it can be concluded that water and surfactant molecules move from the lower to the upper phase with increasing water content. This implies that these spherulites shed numbers of their external layers as they are progressively compressed together.

TABLE 5: Calculated Surfactant and Water Volume Fractions in Various Structures[a]

w	29	30	31	32	33	34	35	36	37	38
$100X_s^{s\cdot fcc}$	31	30	30	29	29	28	28	27	27	27
$100X_s^{s\cdot bcc}$	28	28	27	27	26	26	26	25	25	24
$100X_s^{s\cdot sc}$	22	21	21	21	20	20	20	19	19	19
$100X_s^{s\cdot fcc}$	39	38	37	37	36	35	35	34	34	33
$100X_s^{c\cdot s}$	33	33	32	32	31	31	30	30	29	29
$100X_s^{c\cdot i\cdot c}$	40	39	39	38	37	37	36	35	35	34
$100X_s^{c\cdot i\cdot fcc}$	35	34	34	33	33	32	32	31	31	30
$100X_w^{s\cdot fcc}$	42	42	43	44	44	45	46	46	47	47
$100X_w^{s\cdot bcc}$	38	39	40	40	41	41	42	42	43	43
$100X_w^{s\cdot sc}$	29	30	30	31	31	32	32	33	33	33
$100X_w^{c\cdot hcp}$	52	53	54	55	55	56	57	58	58	59
$100X_w^{c\cdot s}$	45	46	47	47	48	49	49	50	50	51
$100X_w^{c\cdot i\cdot c}$	54	55	56	57	58	58	59	60	60	61
$100X_w^{c\cdot i\cdot fcc}$	48	48	49	50	50	51	52	52	53	53

[a] (i) For spheres: $X_s^{s\cdot fcc}$, $X_w^{s\cdot fcc}$ for fcc; $X_s^{s\cdot bcc}$, $X_w^{s\cdot bcc}$ for bcc; $X_s^{s\cdot sc}$, $X_w^{s\cdot sc}$ for simple cubic. (ii) For cylinders: $X_s^{c\cdot hcp}$, $X_w^{c\cdot hcp}$ for hexagonal; $X_s^{c\cdot s}$, $X_w^{c\cdot s}$ for square; $X_s^{c\cdot i\cdot c}$, $X_w^{c\cdot i\cdot c}$ for interconnected cubic; $X_s^{c\cdot i\cdot fcc}$, $X_w^{c\cdot i\cdot fcc}$ for fcc interconnected cylinders.

TABLE 6: Overall Water Content, *w*, of Region VII[a]

w	29	30	31	32	33	34	35	36	37	38
σ (Å^2)		53		55		55		55		
shape		c		c/s		s			s	
R^s (Å)				60		65		70		
l^c (Å)		104								
$100\phi_s$	22.5	22.2	22	21.8	21.6	21.3	21.1	20.9	20.7	20.5
$100\phi_w$	30.5	31.2	31.9	32.6	33.3	34	34.6	35.3	35.9	36.5
$100\phi_o$	47	46.6	46.1	45.6	45.1	44.7	44.3	43.8	43.4	43
κ (mS)	2.29	2.12	2.09			1.64		1.52	1.42	1.32
ϕ_o/ϕ_s(exp)	2.1	2.1	2.1	2.1	2.1	2.1	2.1	2.1	2.1	2.1
ϕ_o/ϕ_s(cal s)	2.22	2.28	2.31	2.34	2.37	2.41	2.44	2.47	2.51	2.54
ϕ_o/ϕ_s(cal c)	0.64	0.65	0.65	0.66	0.67	0.68	0.69	0.70	0.70	0.71

[a] Head polar area, σ, shape of the objects (cylinders (c) or spheres (s)), polar radius of a spherical droplet, R^s, width of the cylinders, l^c. Surfactant, ϕ_s, water, ϕ_w, and oil, ϕ_o, volume fractions measured. κ is the conductivity; ϕ_o/ϕ_s(cal s) and ϕ_o/ϕ_s(cal c) are the calculated ratio of oil versus surfactant volume fraction for interdigitated spheres and cylinders, respectively. $[Cu(AOT)_2]_0 = 4.2 \times 10^{-1}$ M.

From the theoretical model of section 2, the spherulite interior has to collapse to form interconnected cylinders. This is supported by geometry and energetic considerations. The calculated water volume fraction, X_w (eq 15), obtained by assuming a simple model packing of interconnected cylinders with a fcc structure is given in Table 2. The X_w values are higher than those determined for the isotropic phase, ϕ_w, either in phase V_{b1} or V_{b2}. This discrepancy is due to the fact that the model can claim qualitative validity only. However, the order of magnitude is within the right range. A much better agreement with experiments could easily be achieved by making the reasonable assumption that the connected cylinders have a much looser packing than those assumed in eq 15.

Knowing the lamellar spacing, d, the average thickness of the oil and water layers can be deduced from eq 17. Table 2 shows that the water and oil thickness, L and Δ, decrease with increasing water content. The overall volume fraction of surfactant, Φ_s, water, Φ_w, and oil, Φ_o, deduced from the lamellar spacing determined by SAXS and from the relative volumes of phase V_{b1} and V_{b2} are compared to the measured values determined from titration of $Cu(AOT)_2$ and water. Table 3 shows very good agreement between the surfactant, water, and oil volume fractions calculated and measured. This is remarkable. It shows that macroscopic measurements of phase volume together with titration and a model based only on geometry gives

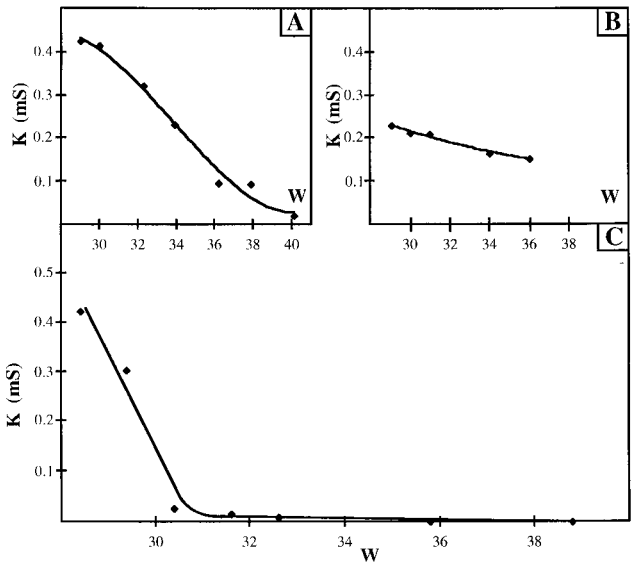

Figure 12. Variation of conductivity of 5×10^{-2} M $Cu(AOT)_2$ in isooctane solution forming phase with increasing water content (A). Inset: Same variation measured at $[Cu(AOT)_2]_0 = 1.2 \times 10^{-1}$ M (B) and $[Cu(AOT)_2]_0 = 4.2 \times 10^{-1}$ M (C).

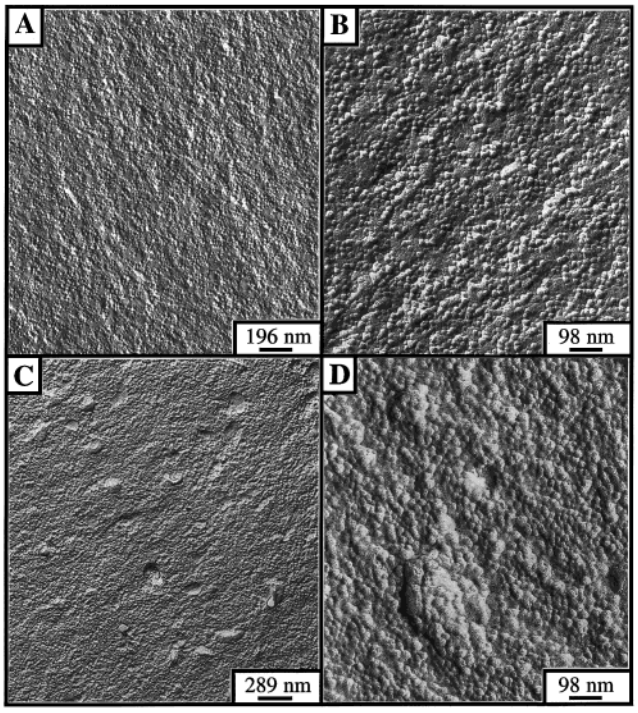

Figure 13. FFEM patterns of the isotropic phase of region VII obtained at $w = 40$ at $[Cu(AOT)_2]_0 = 1.2 \times 10^{-1}$ M ($\phi_s = 0.08$, $\phi_w = 0.14$, $\phi_o = 0.78$) (A, B) and $[Cu(AOT)_2]_0 = 4.2 \times 10^{-1}$ M ($\phi_s = 0.20$, $\phi_w = 0.37$, $\phi_o = 0.43$) (C, D).

an excellent description of microscopic behavior, reflected here in the relative spacing of oil and water. The system is a kind of osmometer.

The discussion above is clearly an oversimplification. Spherulites will obviously be highly polydisperse. The lower phase will contain the largest objects admixed with the connected cylinder phase. The upper phase will have the connected cylinder phase admixed with small spherulites with fewer lamellar bilayers, as can be seen in Figure 8A. If the number of bilayers is small, they will contribute little to the scattering. This interpretation becomes more plausible if we recall that the

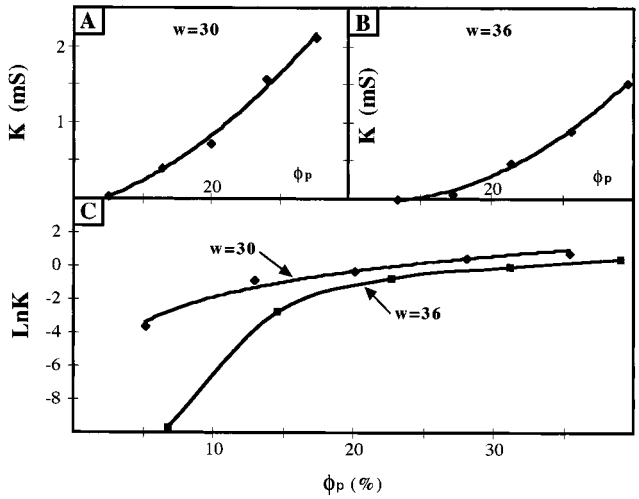

Figure 14. Variation of the conductance with polar volume fraction at $w = 30$ (A) and $w = 36$ (B). Comparison in the log scale of conductance at $w = 30$ and $w = 36$ (C).

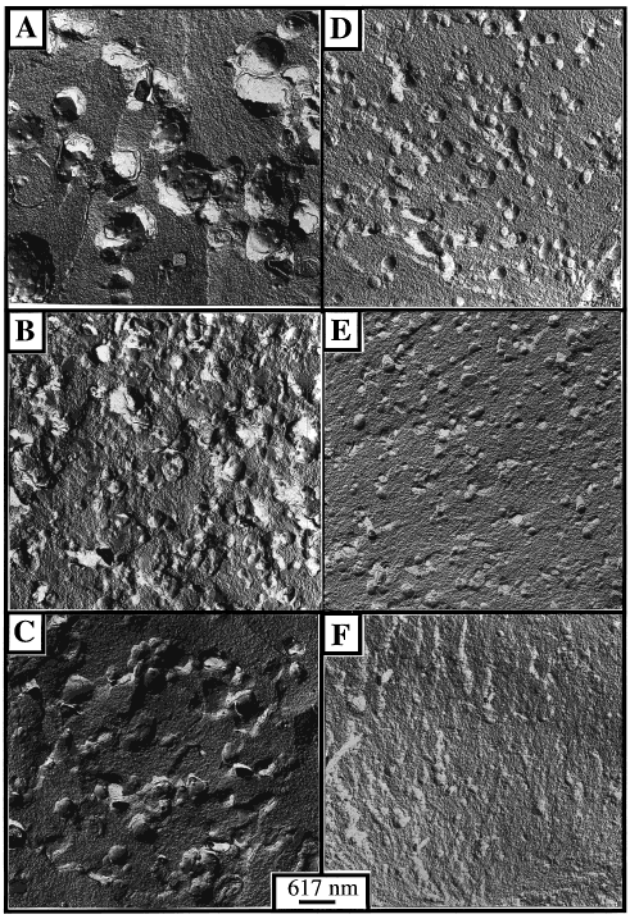

Figure 15. Change of the FFEM patterns of phases VI and VII with the water content at fixed $Cu(AOT)_2$ concentration: $[Cu(AOT)_2]_0 = 4.2 \times 10^{-1}$ M (A) $w = 26.5$ ($\phi_s = 0.23$, $\phi_w = 0.29$, $\phi_o = 0.48$); (B) $w = 28.5$ ($\phi_s = 0.23$, $\phi_w = 0.30$, $\phi_o = 0.47$); (C) $w = 30$ ($\phi_s = 0.22$, $\phi_w = 0.32$, $\phi_o = 0.46$); (D) $w = 32$ ($\phi_s = 0.22$, $\phi_w = 0.33$, $\phi_o = 0.55$); (E) $w = 34$; (F) $w = 36$ ($\phi_s = 0.21$, $\phi_w = 0.36$, $\phi_o = 0.43$).

separation between two phases requires centrifugation or a time of several hours.

Formation of "supra-aggregates" can be accounted for as follows: Above $w = 10$ (region III_t), the polar headgroup is almost totally hydrated and its area is nearly fixed. The binding of copper ions to the interface decreases and the fixed headgroup

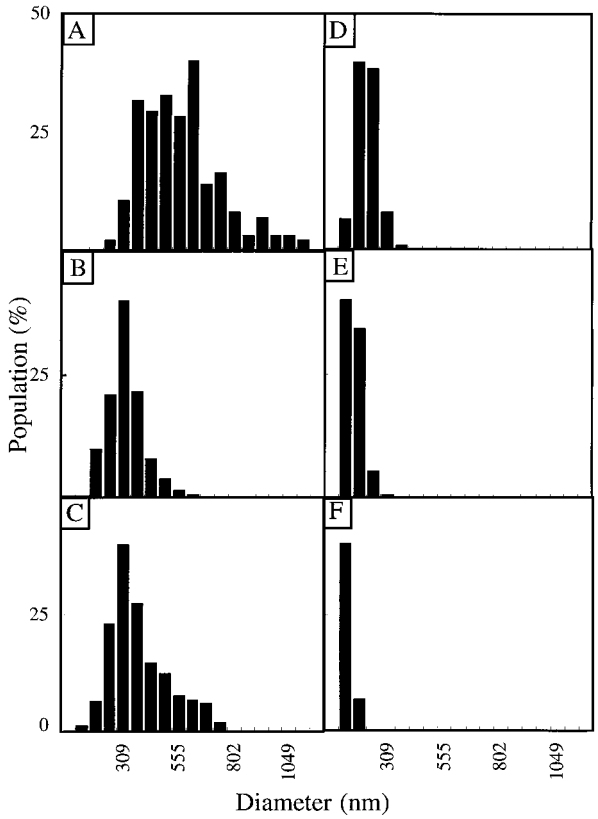

Figure 16. Histograms of the large objects observed in Figure 15.

area set by steric (hydration) interactions also sets oil penetration and optimum curvature for the formation of planar lamellae. With a further increase in water content, the interior (highly curved) bilayers become energetically unfavorable as more and more oil is exposed to the water interface.

This is solely a consequence of geometry and will occur for any topologically closed container. The formation of any multiwalled liposomal like phase is here dictated by global packing constraints, that is when cylinders can no longer pack into a single phase. But the interior becomes energetically unfavorable.

At this point (regions III_t, IV_b, and V_t), the system collapses to a supra-aggregate with isotropic phases outside and inside the spherulites. A further increase in water content induces formation of region V_t. The problem is obviously more complicated. Chemical potentials inside and outside of spherulites must be equal and that additional requirement determines the number of lamellae that will rearrange in the interior and exterior of the supra-aggregate microphase.

A further increase in the water content causes the complete disappearance of the birefringent phase with formation of an isotropic phase in coexistence with isooctane (region VI_b). With an increase in $Cu(AOT)_2$ concentration, the isooctane phase progressively disappears and one isotropic phase is formed (region VI). The FFEM patterns of phase VI_b exhibit rather large objects at low (Figure 11A) and high $Cu(AOT)_2$ concentration (Figure 11B). With a further increase in water content, the isooctane phase progressively decreases until one isotropic phase is reached (region VII).

Structural study has been impracticable because of the small water content range over which phases VI_b and VI exist. We will concentrate on the region VII.

Whatever the $Cu(AOT)_2$ concentration, a slight increase in the water content induces formation of a single isotropic phase

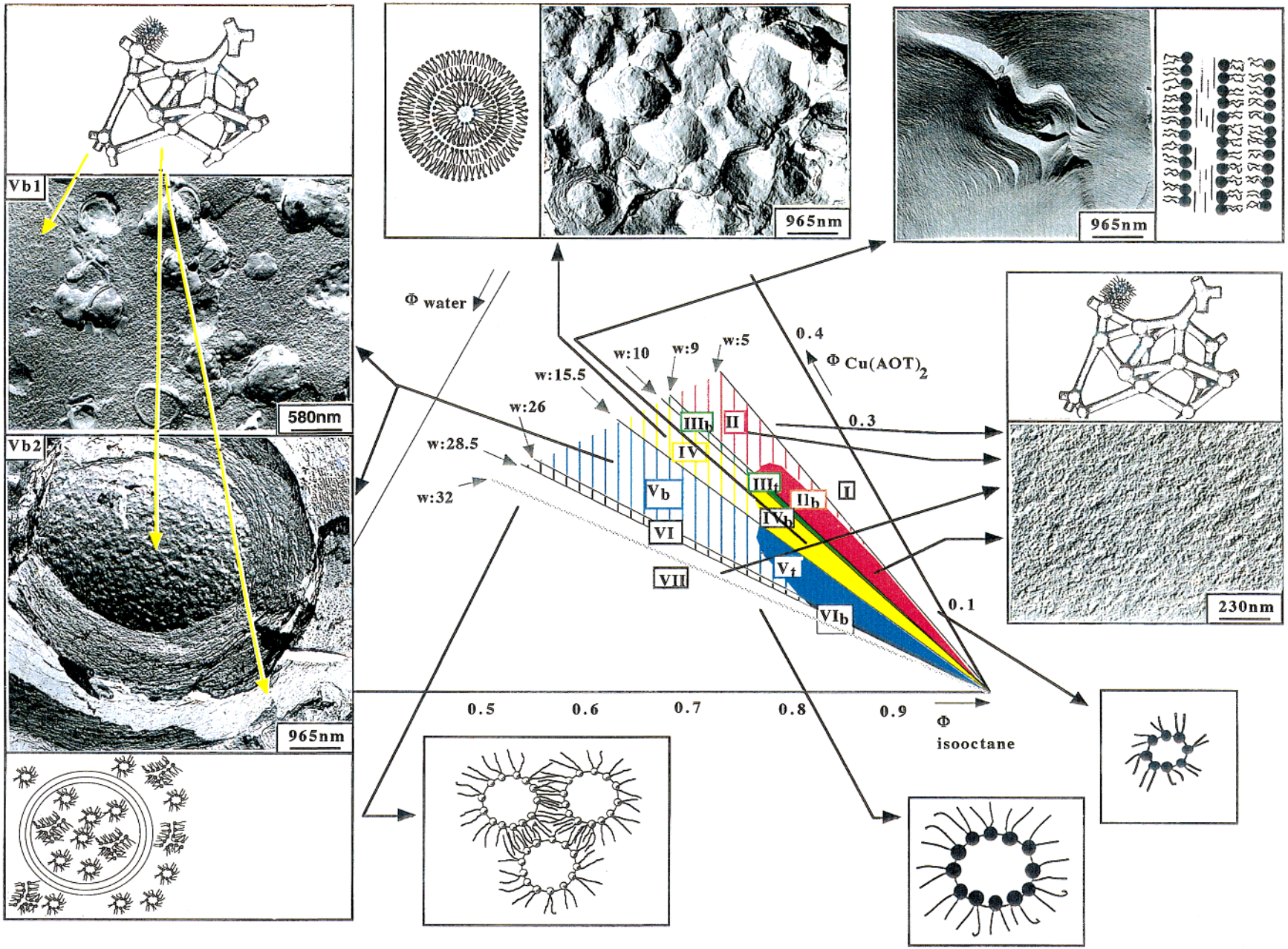

Figure 17. Phase diagram $Cu(AOT)_2$−water−isooctane showing the various structures. The dashed line represents the transition between cylinders and spheres.

region (phase VII). The surfactant and water volume fractions determined experimentally at low (Table 4) and high (Table 6) $Cu(AOT)_2$ concentration are always lower than those calculated (Table 5). This indicates that both cylinders and spheres can pack. However, as mentioned above, this packing does not take into account aggregate interactions.

Conductance measured at various water contents is especially deserving of note (Figure 12). At low $Cu(AOT)_2$ concentration ($[Cu(AOT)_2]_0 = 5 \times 10^{-2}$ M, the conductance is rather large at $w = 28.5$ in the range of milliSiemens. With increasing water content, the conductance dropped markedly to level off at water content up to $w = 33$. The conductance is then in the range of nanoSiemens. This indicates a decrease in the number of connections with increasing water content. At higher $Cu(AOT)_2$ concentrations ($[Cu(AOT)_2]_0 = 1.2 \times 10^{-1}$ M and $[Cu(AOT)_2]_0 = 4.1 \times 10^{-1}$ M) the conductance is also large but still decreases with increasing water content (insets A and B Figure 12).

From SAXS (Tables 4 and Table 6), at relatively low water content ($w = 29$), the scattering is characteristic of cylinders. By $w = 32$, a transition takes place. It is difficult to distinguish between scattering of spheres and cylinders. Probably a mixture of both exists. Above $w = 32$, scattering characteristic of spheres is obtained.

The FFEM patterns at $w = 40$ show, at low surfactant concentration, reverse micelles in the 20−40 nm diameter range (Figure 13A,B).

From these data, it can be concluded that a transition takes place around $w = 32$: Below this water content connected cylinders exist, whereas above $w = 32$ spheres are formed. This is confirmed by the change of the conductivity with polar volume fraction, measured at $w = 30$ and $w = 36$. Figure 14A shows, at $w = 30$, a linear increase in the conductivity with polar volume fraction, ϕ_p. This indicates an increase in the number of connections of the "cylinders". At the opposite extreme, Figure 14B shows, at $w = 36$, a low conductivity at low polar volume fraction. Below, $\phi_p = 0.17$ isolated droplets are dispersed in the solution. At $\phi_p = 0.17$, a percolation onset is observed and the conductivity increases drastically. Comparison on a ln scale of the conductance variation with the polar volume fraction at $w = 30$ and 36 indicates a strong change in microstructure (Figure 13C): At $w = 30$, the conductance increases by 4 orders of magnitude and 10 orders of magnitude at $w = 36$. From these data, it can be concluded that, in phase VII, a transition takes place at $w = 32$. With increasing water content, an antipercolation process takes place, whereas with increasing surfactant a percolation is observed. This is entirely to be expected. We have visualized the complex conductance behavior in terms of connected cylinders and spheres. The headgroup is fully hydrated and curvature at the interface remains constant. With increasing water content, the only solution to the problem of maintaining constant average curvature consistent with global packing is achieved by reducing connections in the network that ultimately becomes disconnected spheres.

Below $w = 32$, interconnected cylinders are formed with an increase in the number of connections on an increase in the surfactant concentration. The surfactant and water volume fractions determined experimentally (Table 4) are always lower than those calculated (Table 5). However, as mentioned above, this packing does not take into account aggregate interactions.

At low surfactant concentration, the ratio of oil to surfactant volume fraction measured and calculated (Table 4) indicates that the alkyl chains have sufficient oil and do not need to interdigitate. In apposition, at high $Cu(AOT)_2$ concentration, there is insufficient oil to solvate the chains (Table 6). This favors the interdigitation of spherical droplets. This is confirmed by the presence of small objects at low $Cu(AOT)_2$ concentration (Figure 13A,B). With increasing $Cu(AOT)_2$ concentration, large objects appear concentrated (Figure 13C,D). These large objects could be attributed to interdigitated reverse micelles.

At high $Cu(AOT)_2$ concentration, the FFEM patterns of regions VI and VII show a puzzling behavior. At low water content ($w = 26.5$), Figure 15A shows large objects in coexistence with smaller ones. The pattern is reminiscent of that observed with the isotropic phase of V_{b1} (Figure 9A). With increasing water content (Figure 15), at fixed $Cu(AOT)_2$ concentration, the size of the large object decreases. The size and polydispersity decrease with increasing water content (Figure 16). Presumably, the dual requirement that the chemical potential of both oil and water inside and outside any topologically closed containers is responsible for this gradual dissolution of these last vestiges of the unfortunate spherulites.

Figure 17 summarizes the various structures determined in the phase diagram.

4. Conclusion

We began this study with a system that exhibited an apparently impossibly complex range of phase behavior. What we have shown is that not just phase behavior but even microstructures can be predicted. Only a little algebra with local and global packing conditions from elementary geometry is sufficient to gain insight. Proportions within different two- and three-phase regions require some extra knowledge of peculiar forces acting in these systems, probably due to conduction processes between cylinders, but not much.

The emergence of supra-aggregates as equilibrium systems and their nature is surprising and as far as we are aware quite new. This is an important issue. It implies that the older idea of a phase within multicomponent fluids containing surfactants as a system with homogeneous microstructure may be too restrictive, likewise for the idea that emulsions are necessarily thermodynamically unstable.

Further, what is also occurring is that these microstructures acting as templates for nanoparticle syntheses produce particles whose structure apparently does coincide with the known liquid template.

Glossary

w	water content
N_w	number of water molecules
N_s	number of surfactant molecules
N_s^i	number of surfactant molecules in the internal layer
N_s^o	number of surfactant molecules in the outer layer
f	volume fraction of a phase
υ_w	volume of water molecules
υ_s	volume of surfactant molecules
a_s	area of polar headgroup
a_s^o	head polar area of the surfactant in the outer layer
a_s^i	head polar area of the surfactant in the outer layer
d	peak to peak spacing of layer, bilayer thickness
l_s	surfactant tail length
l_s^i	internal surfactant tail length
l_s^o	outer surfactant tail length
ϕ_w	water volume fraction
ϕ_s	surfactant volume fraction
ϕ_o	oil volume fraction

Φ_s	bound oil volume fraction
Φs	overall surfactant volume fraction
Φo	overall oil volume fraction
Φw	overall water volume fraction
s	packing parameter
R_w	water pool radius
R	radius of a spherulite
Δ	thickness of free oil in the lamella
L	thickness of water in the lamella
R^s (Å)	polar radius of a spherical droplet
l^c (Å)	average width of cylinders
L^c	average length of cylinders, length of the mean chord length
$X_s^{s\cdot fcc}$	surfactant volume fraction of spheres packed in the fcc structure
$X_s^{s\cdot bcc}$	surfactant volume fraction of spheres packed in the bcc structure
$X_s^{s\cdot sc}$	surfactant volume fraction of spheres packed in the simple cubic structure
$X_s^{c\cdot s}$	surfactant volume fraction of cylinders packed in the square structure
$X_s^{c\cdot hcp}$	surfactant volume fraction of cylinders packed in the hcp structure
$X_s^{c\cdot i\cdot c}$	surfactant volume fraction of cylinders packed in the interconnected cubic structure
$X_w^{c\cdot i\cdot fcc}$	surfactant volume fraction of cylinders packed in the interconnected fcc structure
$X_w^{s\cdot fcc}$	water volume fraction of spheres packed in the fcc structure
$X_w^{s\cdot bcc}$	water volume fraction of spheres packed in the bcc structure
$X_w^{s\cdot sc}$	water volume fraction of spheres packed in the simple cubic structure
$X_w^{c\cdot s}$	water volume fraction of cylinders packed in the square structure
$X_w^{c\cdot hcp}$	water volume fraction of cylinders packed in the hcp structure
$X_w^{c\cdot i\cdot c}$	water volume fraction of cylinders packed in cubic interconnected structure

References and Notes

(1) *Reactivity in Reverse Micelles*; Pileni, M. P., Ed.; Elsevier: Amsterdam, New York, Oxford, Shannon, Tokyo, 1989.

(2) *The language of shape*; Hyde, S., Andersoon, S., Larsson, K., Blum, Z., Landh, T., Lidin, S., Ninham, B. W., Eds.; Elsevier: Amsterdam, New York, Oxford, Shannon, Tokyo, 1997.

(3) Chen, S. J.; Evans, D. F.; Ninham, B. W.; Mitchell, D. J.; Blum, F. D.; Pickup, S. *J. Phys. Chem.* **1986**, *90*, 842.

(4) Evans, D. F.; Mitchell, D. J. Ninham, B. W. *J. Phys. Chem.* **1986**, *90*, 2817.

(5) Barnes, I. S.; Hyde, S. T.; Ninham, B. W.; Derian, P. J.; Drifford, M.; Zemb, T.N. *J. Phys. Chem.* **1988**, *92*, 2286.

(6) Mazer, N.; Benedek, G.; Carey, M. C. *J. Phys. Chem.* **1976,** 80, 1075.

(7) Blankschtein, D.; Thurston, G. M.; Benedek, G. *Phys. Rev. Lett.* **1986**, *85*, 7268.

(8) Porte, G.; Appell, J.; Poggi, Y. *J. Phys. Chem.* **1980**, *84*, 3105.

(9) Hoffmann, H.; Platz, G.; Ulbricht, W. *J. Phys. Chem.* **1981**, *85*, 3160.

(10) Mishic, J. R.; Fisch, M. R. *J. Chem. Phys.* **1990**, *92*, 3222.

(11) Mitchell, D. J.; Ninham, B. W. *J. Chem. Soc., Faraday Trans.* **1981**, *77*, 601.

(12) Safran, S. A.; Turkevich, L. A.; Pincus, P. A. *J. Phys. Lett.* **1984**, *45*, L69.

(13) Talmon, Y.; Prager, S. *J. Chem. Phys.* **1978**, *69*, 2984.

(14) Widom, B. *J. Chem. Phys.* **1984**, *81*, 1030.

(15) Knackstedt, M. A.; Ninham, B. W. *Phys. Rev. E* **1994**, *50*, 2839.

(16) Petit, C.; Lixon, P.; Pileni, M. P. *Langmuir* **1991**, *7*, 2620.

(17) Eastoe, J.; Fragneto, G.; Robinson, B. H.; Towey, T. F.; Heenan, R. K.; Leng, F. J. *J. Chem. Soc., Faraday Trans.* **1992**, *88* (3), 461.

(18) Eastoe, J.; Steytler, D. C.; Robinson, B. H.; Heenan, R. K.; North, A. N.; Dore, J. C. *J. Chem. Soc., Faraday Trans.* **1994**, *90* (17), 2479.

(19) Eastoe, J.; Robinson, B. H.; Heenan, R. K. *Langmuir* **1993**, *9*, 2820.

(20) Eastoe, J.; Towey, T. F.; Robinson, B. H.; Williams, J.; Heenan, R. K. *J. Phys. Chem.* **1993**, *97*, 1459.

(21) Fioretto, D.; Freda, M.; Mannaioli, S.; Oniri, G.; Santucci, A. *J. Phys. Chem.* **1999**, *103*, 2631.

(22) Tanori, J.; Gulik, T.; Pileni, M. P. *Langmuir* **1997**, *13*, 632.

(23) Pileni, M. P. *J. Phys. Chem.* **1993**, *97*, 6961.

(24) Pileni, M. P. *Langmuir* **1997**, *13*, 3266.

(25) Lisiecki, I.; Pileni, M. P. *J. Am. Chem. Soc.* **1993**, *115*, 3887.

(26) Lisiecki, I.; Pileni, M. P. *J. Phys. Chem.* **1995**, *99*, 5077.

(27) Tanori, J.; Pileni, M. P. *Adv. Mater.* **1995**, *7*, 862.

(28) Tanori, J.; Pileni, M. P. *Langmuir* **1997**, *13*, 639.

(29) Tanori, J.; Filemkembo, A.; Gulik, T.; Pileni, M. P. *Langmuir* **1998**, *14*, 632.